Progress In Electromagnetics Research C, Vol. 90, 51–63, 2019

A New Fast and Accurate Compressive Sensing Technique for Magnetic Resonance Image

Huihui Yue and Xiangjun Yin*

Abstract—In this paper, the main problem to be solved is how to achieve magnetic resonance imaging (MRI) accurately and quickly. Previous work has shown that compressive sensing (CS) technology can reconstruct a magnetic resonance (MR) image from only a small number of samples, which significantly reduces MR scanning time. Based on this, an algorithm to improve the accuracy of MRI, called regularized weighting Composite Gaussian smoothed ℓ_0-norm minimization (RWCGSL0), is proposed in this paper. Different from previous methods, our algorithm has three influential contributions: (1) a new smoothed Composite Gaussian function (CGF) is proposed to be closer to the ℓ_0-norm; (2) a new weighting function is proposed; (3) a new ℓ_0 regularized objective function framework is constructed. Furthermore, the optimal solution of this objective function is obtained by penalty decomposition (PD) method. It is experimentally shown that the proposed algorithm outperforms other state-of-the-art CS algorithms in the reconstruction of MR images.

1. INTRODUCTION

MRI plays an essential role in clinical diagnosis and is a medical imaging technique which uses strong magnetic fields and radio waves to produce images of human body, but the process of MRI data acquisition is limited by the following factors: [1]

- It is inconvenient for patients to collect information of their physical condition by long-time scanning.
- Too many samples need a lot of storage space, so these samples need to be compressed.
  Therefore, how to reconstruct an MR image with good quality from only a small number of measurements (that is, to restore the MR image accurately by undersampling) has become a widespread concern. It can significantly shorten MR scanning time and reduce storage space. Recent developments in CS [2–4] have shown that it is possible to realize this idea. As a theory to solve the underdetermined linear inverse problem, CS can seek an approximate sparse solution (which has only a few non-zero values) of a linear system. In other words, CS technology can accurately reconstruct the original sparse vector with less sampling, thereby reducing the storage space and shortening the scanning time. So CS technology can be successfully applied to MRI when the following two conditions are satisfied:
- Medical images can be converted to sparse images by proper transformation.
- MRI scanners generally obtain samples in encoded form.
  In fact, MR images can be sparsely represented by appropriate basis such as DCT, Fourier, Wavelet Curvelet, and Gabor [5]. MR image is constructed by collecting a sequence of frames of data, called *acquisitions* [6]. So the above two conditions can be satisfied. Furthermore, the application of CS in MRI has attracted worldwide attention.

Received 17 October 2018, Accepted 13 January 2019, Scheduled 11 February 2019
* Corresponding author: Xiangjun Yin (yinxiangjun@hrbeu.edu.cn).
The authors are with the College of Information and Communication Engineering, Harbin Engineering University, Harbin 150001, China.

For CS, its core algorithms are some families of matching pursuit and optimization classes. Matching pursuit algorithms are effective sparse reconstruction methods, such as OMP [7], GOMP [8], CoSaMP [9], and SP [10]. Although these algorithms can accurately reconstruct the original sparse vector, they need known vector sparsity as a priori information and are sensitive to noise, which limits their application in MR image reconstruction. Basis pursuit (BP) is a class of representative optimization algorithms, which is based on constrained ℓ_1-norm minimization [11]. The BP algorithm makes it a problem of linear programming which solves problem by polynomial equation. However, the performance of BP algorithm is also poor in noise environment. Since the smoothed function to approach ℓ_0-norm (SL0) is proposed [12, 13], CS can be well applied in MRI. SL0 is a fast algorithm based on overcomplete sparse decomposition, which can directly minimize the ℓ_0-norm. It has a reconstruction speed of 2 to 3 times faster than the BP algorithm with the same or higher accuracy. Based on SL0, Wang et al. proposed the Thresholded SL0 (TSL0) [14], Ghalehjegh et al. proposed the Block SL0 (BSL0) [15], and Zhao et al. proposed Newton SL0 (NSL0) [16]. These methods give adequate consideration on sparsity and convergence of the solution, but they are unstable in a noisy environment. Based on this, the ℓ_2-SL0 [17–19] transformed the ℓ_0-norm problem into the regularized least squares problem (LSP) [20], which includes sparsity regularizer and deviation term, to improve the performance of sparse vector recovery under noisy conditions. Further, ℓ_p-RLS [21] that converts the sparsity regularizer into ℓ_p-norm is introduced to effectively reduce the computational complexity. The ℓ_2-SL0 algorithm and ℓ_p-RLS algorithm both improve the performance of sparse vector recovery under noise conditions and become more effective sparse signal reconstruction methods at present, which make CS better applied in MR image reconstruction. However, the common defect of these two algorithms is their limited reconstruction accuracy.

Based on all the popular algorithms mentioned above, this paper proposes RWCGSL0 algorithm to improve the accuracy of signal and MR image reconstruction under noisy conditions. The core of this algorithm is to achieve a further approximation of the ℓ_0-norm [22] with a new smoothed CGF and combine it with a weighting function to promote sparsity and speed up convergence. Meanwhile, the objective function is obtained by regularization mechanism which can suppress noise in ℓ_2-SL0 and ℓ_p-RLS algorithms. Furthermore, PD method is performed to optimize the process of approximating the optimal solution.

The rest of this paper is organized as follows. Section 2 reviews the basic theoretical background of MRI and CS technology. Then the theories of RWCGSL0 is introduced in Section 3. In Section 4, the performance of the RWCGSL0 algorithm is verified through simulation experiments, and this algorithm is applied to MRI. Section 5 concludes this paper.

2. BACKGROUND

The undersampling process in MRI can be expressed as

$$\mathbf{y} = \boldsymbol{\psi}\boldsymbol{\varphi}\mathbf{x} + \mathbf{b} \tag{1}$$

where $\mathbf{y} \in \mathbb{R}^m$ is the acquired data from the scanner called as k-space MRI data, and $\mathbf{x} \in \mathbb{R}^n$ is the MR image rearranged to a column vector, $m \ll n$. $\boldsymbol{\psi} \in \mathbb{R}^{m\times n}$ represents a random undersampling matrix, and $\boldsymbol{\varphi} \in \mathbb{R}^{n\times n}$ represents the sparse basis matrix that MR mapped to it can be sparse. $\mathbf{b} \in \mathbb{R}^m$ denotes noise that obeys a Gaussian distribution. Therefore, the key problem to be solved in MRI is to accurately reconstruct the original MR from an underdetermined system of linear equation (USLE).

In essence, the CS theory is to solve an underdetermined linear inverse problem, which seeks an approximate sparse solution to a linear system. The model of CS is

$$\mathbf{y} = \boldsymbol{\Phi}\mathbf{x} + \mathbf{b} \tag{2}$$

where $\boldsymbol{\Phi} = \boldsymbol{\psi}\boldsymbol{\varphi} \in \mathbb{R}^{m\times n}$, which can be further represented as $\boldsymbol{\Phi} = [\boldsymbol{\phi}_1, \boldsymbol{\phi}_2, \ldots, \boldsymbol{\phi}_n]$, $\boldsymbol{\phi}_i \in \mathbb{R}^m, i = 1, 2, \ldots, n$. $\boldsymbol{\psi}$ and $\boldsymbol{\varphi}$ as shown in Eq. (1). Eq. (2) can be interpreted as a sparse constraint problem [23–25] with relaxing the equality constraint to allow some error tolerance $\varepsilon \geq 0$:

$$\arg\min_{\mathbf{x}\in\mathbb{R}^n} ||\mathbf{x}||_0 \quad s.t. \quad ||\boldsymbol{\Phi}\mathbf{x} - \mathbf{y}||_2 \leq \varepsilon \tag{3}$$

where $||\cdot||_0$ is ℓ_0-norm, which represents the number of nonzero elements in a vector. We can use a parameter $\lambda > 0$ to balance the twin objectives of minimizing both error and sparsity, and reformulate Equation (3) as the regularized LSP

$$\arg\min_{\mathbf{x}\in\mathbb{R}^n} \frac{1}{2}||\mathbf{\Phi x} - \mathbf{y}||_2^2 + \lambda||\mathbf{x}||_0. \tag{4}$$

Unfortunately, solving $||\mathbf{x}||_0$ in Equations (3) and (4) is an NP-hard problem, and its computational complexity grows geometrically with respect to the signal size. In order to solve this problem, the state-of-the-art algorithms replace $||\mathbf{x}||_0$ with $h(\mathbf{x})$

$$\arg\min_{\mathbf{x}\in\mathbb{R}^n} \frac{1}{2}||\mathbf{\Phi x} - \mathbf{y}||_2^2 + \lambda h(\mathbf{x}). \tag{5}$$

Now, our goal is to solve Equation (5) using the RWCGSL0 algorithm.

3. THE PROPOSED RWCGSL0 ALGORITHM

3.1. Related Work

In this section, On the basis of Eq. (5), we proposed a new ℓ_0 smoothed function, and therefore, a new ℓ_0 regularized objective function framework is proposed and shown as follows,

$$\arg\min_{\mathbf{x}\in\mathbb{R}^n} \frac{1}{2}||\mathbf{y} - \mathbf{\Phi x}||_2^2 + \lambda \mathbf{W} \sum_{i=1}^{n} \left(1 - \frac{2}{1 + e^{x_i^2/\sigma^2}}\right) \tag{6}$$

where $\mathbf{W}$ is the weighting function, $1 - \frac{2}{1+e^{x_i^2/\sigma^2}}$ the smoothed CGF proposed in this paper, and σ a smoothed parameter that determines the quality of the approximation. Let $f_\sigma(x_i) = (1 - \frac{2}{1+e^{x_i^2/\sigma^2}})$, and we can know that $\lim_{\sigma\to 0} f_\sigma(x_i) = \begin{cases} 0 & if\ x_i = 0 \\ 1 & if\ x_i \neq 0 \end{cases}$, and the ℓ_0-norm can be expressed as $||\mathbf{x}||_0 \approx F_\sigma(\mathbf{x}) = \lim_{\sigma\to 0} \sum_{i=1}^{n} f_\sigma(x_i)$ as proof by **Theorem 1**.

Theorem 1. *Let $\chi_i \subseteq R$ and ϕ_i: $R \to R$ for $i = 1, \ldots n$ be given. Suppose that r is a positive integer and $0 \in \chi_i$ for all i. Consider the following ℓ_0-norm minimization problem:*

$$\min \phi(\mathbf{x}) = \sum_{i=1}^{n} \phi_i(x_i) : \ ||\mathbf{x}||_0 \leq r, \quad \mathbf{x} \in \chi_1 \times \ldots \times \chi_n. \tag{7}$$

Let $\tilde{x}_i^* \in argmin\ \{\phi_i(x_i) : x_i \in \chi_i\}$ and $\boldsymbol{I}^* \subseteq \{1, \ldots, n\}$ be the index set corresponding to r largest values of $\{v_i^*\}_{i=1}^n$, where $v_i^* = \phi_i(0) - \phi_i(\tilde{x}_i^*)$ for $i = 1, \ldots n$. Then, $\boldsymbol{x}^*$ is an optimal solution of problem in Eq. (6), where $\boldsymbol{x}^*$ is defined as:

$$x_i^* = \begin{cases} \tilde{x}_i^* & \text{if } i \in \mathbf{I}^* \\ 0 & \text{otherwise} \end{cases} \quad i = 1, \ldots, n. \tag{8}$$

Therefore, the ℓ_0-norm can be approximated by the smoothed function $f_\sigma(x_i)$ when $\sigma \to 0$, which smartly solves the NP-hard problem led by ℓ_0-norm. In order to make a clear and scientific explanation, we conduct the simulation of the new CGF and compare it with the state-of-the-art functions: Gaussian function in ℓ_2-SL0 algorithm [17] and $||x_i||_{p,\epsilon}^p$ in ℓ_p-RLS algorithm [21], as shown in Fig. 1 (when $\sigma = 0.1$, $p = 0.5$ and $\mathbf{x} \in [-0.5, 0.5]$).

Figure 1 displays that the "steeper" the smoothed function is, the closer its value is to the ℓ_0-norm. Obviously, the CGF is "steeper" than the Gaussian function and $||x_i||_{p,\epsilon}^p$. So the CGF has better performance in approximating the ℓ_0-norm.

$\mathbf{W} = [w_1, w_2, \cdots, w_n]$ is given to solve the problem that converges slowly, in which

$$w_i = \frac{1}{e^{x_i^2}}, \quad i = 1, 2, \ldots, n. \tag{9}$$

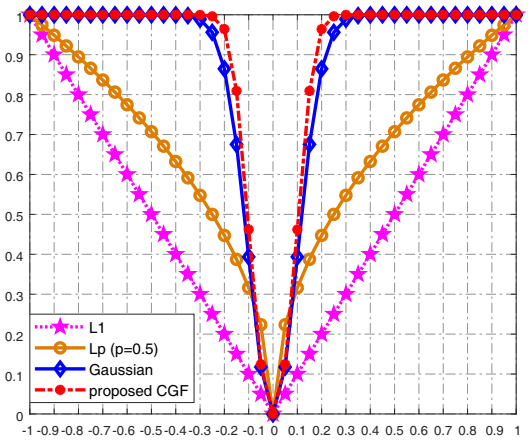

Figure 1. Different smoothed functions are plotted in this figure for $\sigma = 0.1$, and displays ℓ_1-norm of 2D for comparison.

where $w_i \in [0,1]$ is an even function that monotonically decreases on $x_i \in [0,\infty)$, so it has maximum at $x_i = 0$ and minimum at $x_i \to +\infty$ or $x_i \to -\infty$. When $\mathbf{W}$ is added to $F_\sigma(\mathbf{x})$, the large entries in $\mathbf{W}$ could be used to discourage nonzero entries in the recovered signal, while the small entries in $\mathbf{W}$ could be used to encourage nonzero entries. Therefore, compared with popular algorithms that do not consider the weighting strategy (namely, these algorithms are weighting $f_\sigma(x_i)$ with a same value: $w_i = 1$) [27], the combination of $\mathbf{W}$ and $F_\sigma(\mathbf{x})$ leads to a sparse solution faster in the process of optimization [28].

3.2. Optimization by the PD Method of the Proposed RWCGSL0 Algorithm

In this section, we will introduce the PD [29] method to solve the problem in Eq. (6), and Eq. (6) is rewritten as

$$\arg\min_{\mathbf{x}\in\mathbb{R}^n} \frac{1}{2}||\mathbf{y} - \mathbf{\Phi}\mathbf{x}||_2^2 + \lambda \mathbf{W} F_\sigma(\mathbf{x}) \tag{10}$$

where $F_\sigma(\mathbf{x}) = \sum_{i=1}^{n}(1 - \frac{2}{1+e^{x_i^2/\sigma^2}})$. Through the idea of [26], we can reformulate Eq. (10) as follows

$$\arg\min_{\mathbf{x}\in\mathbb{R}^n} \frac{1}{2}||\mathbf{y} - \mathbf{\Phi}\mathbf{x}||_2^2 + \sum_i \lambda H_\sigma(\mathbf{x}) \tag{11}$$

The PD method uses the ℓ_0-norm to constrain the wavelet frame coefficients to make the deconvolution as a regular term, so that the sharp features and smoothness of the acquired signal are balanced. Lu and Zhang [26] proposed the model in Equation (12) for solving the minimum of the ℓ_0-norm by the PD algorithm:

$$\min_{\mathbf{u}\in\mathbf{U}} f(\mathbf{u}) + \alpha||\mathbf{u}_\mathbf{P}||_0 \tag{12}$$

where $\mathbf{U} \in \mathbb{R}^n$, $f : \mathbb{R}^n \to \mathbb{R}$ is a continuous integrable function, and $\alpha > 0$, $||\mathbf{u}_\mathbf{P}||_0$ represents the cardinality from the $\mathbf{P}$ index to the $\mathbf{u}$ subvector. Let $\mathbf{u} = (\mathbf{x}_1,\ldots,\mathbf{x}_n,\mathbf{H}_1,\ldots,\mathbf{H}_m)$, $\mathbf{P} = \{n+1,\ldots,n+m\}$, $\bar{\mathbf{P}} = \{1,\ldots,n\}$, $f(\mathbf{u}) = \frac{1}{2}||\mathbf{y} - \mathbf{\Phi}\mathbf{u}_{\bar{\mathbf{P}}}||_2^2$, $\mathbf{U} = \{\mathbf{u} \in \mathbb{R}^{n+m} : \mathbf{u}_\mathbf{P} = \mathbf{W}\mathbf{u}_{\bar{\mathbf{P}}}\}$, problem in Eq. (10) can be directly converted to Equation (11). In this case, we can use the PD method to directly solve the deconvolution problem.

In order to better solve this optimization problem, the penalty term ϱ is added to Eq. (10), and then the block coordinate descent (BCD) method is used to solve the minimization problem of each sub-problem in the PD method. The model for implementing the optimization process of the RWCGSL0 algorithm with the PD method is as follows:

$$\iota_\varrho(\mathbf{x}, H_\sigma(\mathbf{x})) := \frac{1}{2}||\mathbf{y} - \mathbf{\Phi}\mathbf{x}||_2^2 + \sum_i \lambda H_\sigma(\mathbf{x}) + \frac{\varrho}{2}||\mathbf{W}F_\sigma(\mathbf{x}) - H_\sigma(\mathbf{x})||_2 \tag{13}$$

In addition, the process that the smoothed function $F_\sigma(\mathbf{x})$ gradually approaches the ℓ_0-norm can be accomplished by using a sequential σ-*continuation* strategy. Given σ a small target value σ_T, and a sufficiently large initial value of parameters σ_1, monotonically decreasing sequence $\{\sigma_t | t = 2, 3, \ldots, T\}$ is generated as

$$\sigma_t = \sigma_1 e^{-\gamma(t-1)}, \quad and \quad t = 2, 3, \ldots, T \tag{14}$$

where $\gamma = \frac{log(\sigma_1/\sigma_T)}{T-1}$, and T is the maximum of iterations.

Based on these, we summarize the steps of the RWCGSL0 algorithm as shown in Table 1.

Table 1. Regularized weighting composite gaussian smoothed l_0-norm minimization (RWCGSL0) algorithm using PD method.

Input: $\mathbf{\Phi}$, $\mathbf{x}$, $\mathbf{y}$, $\mathbf{b}$, σ_1, σ_T, T, λ and $\mathbf{x}^* = 0$
Step1: Compute $\mathbf{W}$ using (9), σ_t for $t = 2, 3, \ldots, T-1$ using (14);
Step2: For $t = 1, 2, \ldots, T$
1) Set $\sigma = \sigma_t$, $\tau = 0$, $\mathbf{x}_{(\tau)} = \mathbf{x}^*$, $\delta > 1$, $\varrho^0 > 0$, $\mathbf{H}^0 = 0$, $q = 0$
2) While does not meet the termination criteria of the BCD method
a) $q = q + 1$
b) Compute $\mathbf{x}^{\tau,q} \in \arg\min_{\mathbf{x}} \ \iota_{\varrho\tau}(\mathbf{x}, \mathbf{H}^{\tau,q-1})$
c) Compute $\mathbf{H}^{\tau,q} \in \arg\min_{\mathbf{H}} \ \iota_{\varrho\tau}(\mathbf{x}^{\tau,q-1}, \mathbf{H})$
3) If $(\mathbf{x}^\tau, \mathbf{H}^\tau)$ satisfies the termination condition set in the PD
set $\mathbf{x}^* = \mathbf{x}_\tau$
else
$\delta^{\tau+1} := \ \delta^\tau$
$\tau = \tau + 1$
Step3: Output $\mathbf{x} = \mathbf{x}^*$

As shown in Table 1, $\lambda = 0.1\lambda_{\max}$ and $\lambda_{\max} = 2||\mathbf{\Phi}^T\mathbf{y}||_\infty$ are the same as the values in [30]. As for σ, it can be shown that function $F_\sigma(\mathbf{x})$ remains convex in the region where the largest magnitude of the component of $\mathbf{x}$ is less than σ. Based on this, a reasonable initial value of σ can be chosen as $\sigma_1 = \max(|x_i|) + \tau$ to ensure the optimization starts in a convex region. This greatly facilitates the convergence of the RWCGSL0 algorithm.

4. NUMERICAL SIMULATION AND ANALYSIS

In this section, we will verify the performance of the RWCGSL0 algorithm in the case of noise and apply the algorithm to MRI. The numerical simulation platform is MATLAB 2017b, which is installed on the WINDOWS 10, 64-bit operating system. The CPU is Inter (R) Core (TM) i5-3230M, and the frequency is 2.6 GHz.

First, we analyze the reconstruction performance of the proposed RWCGSL0 algorithm, including *normlized mean square error* (NMSE) and *signal to noise ratio* (SNR). The NMSE is defined as $||\mathbf{x} - \hat{\mathbf{x}}||_2/||\mathbf{x}||_2$, and the SNR is defined as $20\log(||\mathbf{x} - \hat{\mathbf{x}}||_2/||\mathbf{x}||_2)$. In order to visually display this performance, we choose the SL0 [12, 13], ℓ_2-SL0 [17–19] and ℓ_p-RLS [21] algorithms for comparison.

Further, we apply the proposed RWCGSL0 algorithm to recover MRI. For MRI recovery, *Peak Signal to Noise Ratio* (PSNR) and *Structural Similarity Index* (SSIM) are employed to valuate the anti-noise performance and reconstruction similarity performance of RWCGSL0 algorithm, respectively. PSNR is defined as

$$\text{PSNR} = 10\log(255^2/\text{MSE}) \tag{15}$$

where MSE $= ||\mathbf{x} - \widehat{\mathbf{x}}||_2^2$, and SSIM is defined as

$$\text{SSIM}(p,q) = \frac{(2\mu_p + \mu_q + c_1)(2\sigma_{pq} + c_2)}{(\mu_p^2 + \mu_q^2 + c_1)(\sigma_p^2 + \sigma_q^2 + c_2)}. \tag{16}$$

where μ_p is the mean of image p, μ_q the mean of image q, σ_p the variance of image p, σ_q the variance of image q, and σ_{pq} the covariance between image p and image q. Parameters $c_1 = z_1 L$ and $c_2 = z_2 L$, in which $z_1 = 0.01$, $z_2 = 0.03$, and L is the dynamic range of pixel values. Range of SSIM is $[-1, 1]$, and when these two image are same, the SSIM equals 1.

4.1. The Performance Verification of RWCGSL0 Algorithm

For the performance verification experiments, we firstly fix $n = 256$, $m = 100$ and vary the sparsity k (the number of nonzero entries in $\mathbf{x}$) from 1 to 71 at the interval of 5. For each experiment, we randomly generate 100 pairs of $\{\mathbf{x}, \mathbf{\Phi}, \mathbf{b}\}$: the nonzero positions of the sparse signal $\mathbf{x} \in \mathbb{R}^n$ are generated by Gaussian distribution $\mathcal{N}(0,1)$ and the nonzeros entries valued 1; $\mathbf{\Phi}$ is a $m \times n$ random Gaussian matrix with normalized and centralized rows; $\mathbf{b}$ is randomly formed and follows the Rayleigh distribution of $\mathcal{R}(0, \xi)$.

Given the measurement vector $\mathbf{y} = \mathbf{\Phi x} + \mathbf{b}$, the sensing matrix $\mathbf{\Phi}$ and noise $\mathbf{b}$, we try to recover signal $\mathbf{x}$. If $||\mathbf{x} - \widehat{\mathbf{x}}||_2 / ||\mathbf{x}||_2 < 10^{-3}$, the recovery is considered to be a success. The parameters are selected to obtain the best performance for each method: for the SL0 algorithm, $\sigma_{\min} = 10^{-2}$, and scale factors are set as $S = 5$, $\rho = 0.8$; for the ℓ_2-SL0 algorithm, $\sigma_{\min} = 0.01$, $S = 10$, $\rho = 0.8$; for the ℓ_p-RLS algorithm, $p_1 = 1$, $p_T = 0.1$, $\epsilon_1 = 1$, $\epsilon_T = 10^{-2}$; and for the RWCGSL0 algorithm, $\sigma_T = 10^{-2}$. Based on the 100 trials, we compute the NMSE of the above algorithms and plot it in Fig. 2.

From Fig. 2 we can see that the NMSE of all the selected algorithms increases with the increase of k, but the RWCGSL0 algorithm always obtains the smallest NMSE when $k < 50$. This indicates that the RWCGSL0 algorithm has the most accurate recovery performance among all algorithms when the compression ratio (m/n) is within an appropriate range.

We next try to recover the sparse signal $\mathbf{x}$ from a noisy measurement vector $\mathbf{y}$ with different noise intensities ξ, that is input SNR. Specifically, we fix $n = 256$, $m = 100$, $k = 20$ and increase the input SNR. We randomly generate 100 triples of $\{\mathbf{x}, \mathbf{\Phi}, \mathbf{b}\}$. The average SNRs of the recovered signals are shown in Fig. 3. From this figure we can see that the RWCGSL0 approach performs better than the other three approaches. This shows that the RWCGSL0 approach has the best anti-noise performance.

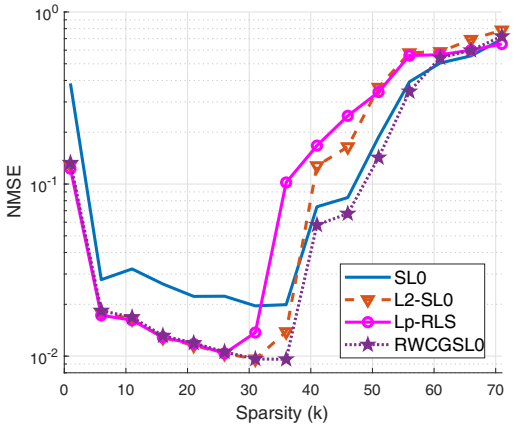

Figure 2. Signal NMSE analysis for SL0, ℓ_2-SL0, ℓ_p-RLS algorithms and proposed RWCGSL0 algorithm with sparsity k from 1 to 71 at the interval of 5, while 100 runs in the noise case $\xi = 0.1$.

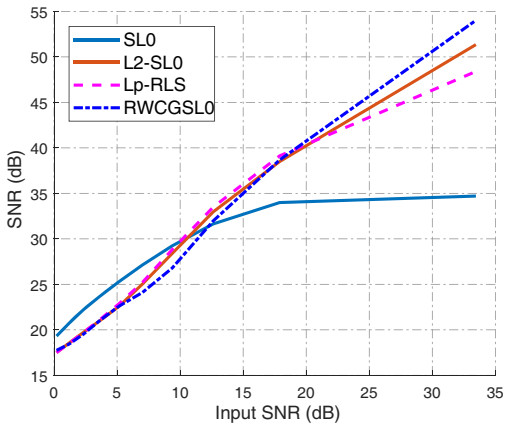

Figure 3. Signal SNR analysis for SL0, ℓ_2-SL0, ℓ_p-RLS algorithms and proposed RWCGSL0 algorithm with input SNR from 0 dB to 35 dB while 100 runs.

Through the above simulation experiments, we prove that the RWCGSL0 algorithm has good recovery accuracy and noise resistance, which provides a basis for the application of the RWCGSL0 algorithm in MRI.

4.2. Application of RWCGSL0 Algorithm in MRI

MR image is considered approximately sparse under some proper basis, such as the DCT basis and DWT basis. Here we compare the recovery performances of the forementioned sparsity approaches based on the real image in Fig. 4. Specifically, in order to reveal the sparse coefficients $\mathbf{x}$ of the real image $\boldsymbol{\Delta}$, we use a DWT basis $\mathbf{V}$: $\boldsymbol{\Delta} = \mathbf{V}\mathbf{x}$, and $\mathbf{x} = \mathbf{V}^T\boldsymbol{\Delta}$. The noisy measurement $\mathbf{y}$ is obtained as follows:

$$\mathbf{y} = \boldsymbol{\psi}\boldsymbol{\Delta} + \mathbf{B} = \boldsymbol{\psi}\mathbf{V}\mathbf{x} + \mathbf{B} = \boldsymbol{\Phi}\mathbf{x} + \mathbf{B}. \tag{17}$$

where $\boldsymbol{\psi}$ represents a random undersampling matrix, $\boldsymbol{\Phi} = \boldsymbol{\psi}\mathbf{V}$. The entries of the noise $\mathbf{B}$ are generated using i.i.d. Rayleigh distribution $\mathcal{R}(0, \xi)$. Taking the RWCGSL0 algorithm, we have the following recovery problem:

$$\arg\min_{\boldsymbol{\Delta}} \frac{1}{2}||\mathbf{y} - \boldsymbol{\Phi}\boldsymbol{\Delta}||_2^2 + \lambda \mathbf{W} F_\sigma(\mathbf{V}^T\boldsymbol{\Delta}) \tag{18}$$

Since the image recovery model has been established as Equation (18), we try to recover the MR image $\boldsymbol{\Delta}$ from a noisy measurement vector $\mathbf{y}$. We firstly fix $\xi = 0.01$ and vary the *compression ratio* (CR) $\in$ [0.10.20.30.40.50.6], and CR is defined as m/n. The recovered MR images by different approaches are shown in Figs. 5–10, and scientific data are shown in Table 2.

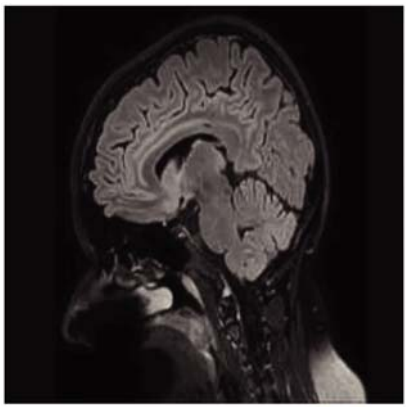

Figure 4. Original MR image (256×256).

Table 2. PSNR and SSIM of recovery images by SL0, ℓ_2-SL0 and ℓ_p-RLS algorithms and proposed RWCGSL0 algorithm.

CR	PSNR (dB)				SSIM (%)			
	SL0	ℓ_2-SL0	ℓ_p-RLS	RRCGSL0	SL0	ℓ_2-SL0	ℓ_p-RLS	RRCGSL0
0.1	10.4181	11.8908	11.4916	12.2672	9.4	11.21	12.90	14.65
0.2	14.7935	14.6812	14.3427	16.5095	47.42	51.43	53.35	68.29
0.3	24.2354	24.4376	24.5534	24.8979	94.52	94.81	94.97	95.40
0.4	26.0331	26.2983	26.4491	27.1441	96.47	96.67	96.79	97.28
0.5	27.2542	27.5049	27.6154	28.6093	97.24	97.38	97.35	97.46
0.6	27.8599	27.9762	28.2383	29.9468	97.69	97.75	97.82	98.56

As shown in Figs. 5–10, when the CR exceeds 0.5, all algorithms can clearly recover the MR image, which fully confirms the feasibility of CS technology in MRI. Further, from the scientific data shown in Table 2, we can see that the RWCGSL0 algorithm has better PSNR and SSIM than other three selected algorithms, which verifies the good MR image recovery performance of proposed RWCGSL0 algorithm.

We next fix CR to 0.5 and analyze MR image recovery effects of the RWCGSL0 algorithm at $\xi = [0, 0.05, 0.1, 0.2, 0.5]$. In order to better show the performance of the proposed RWCGSL0 algorithm, we compare it with the ℓ_p-RLS algorithm. The recovered MR images by the ℓ_p-RLS algorithm and

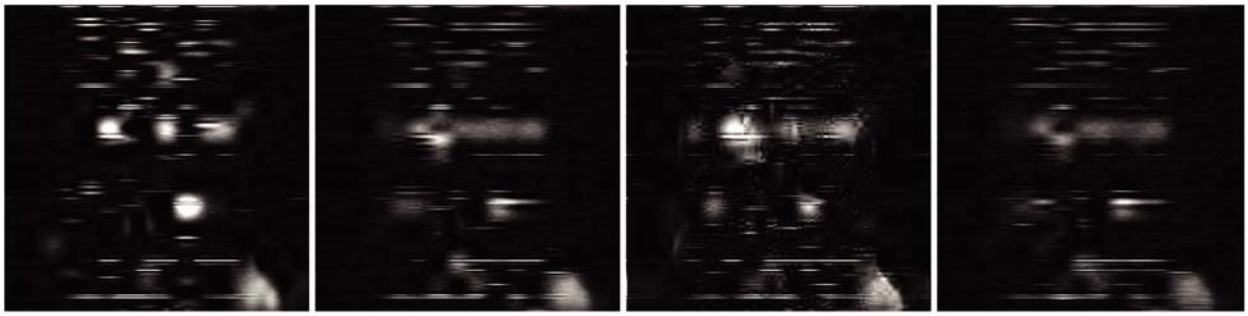

Figure 5. MR image recovery effect with $CR = 0.1$. From left to right, first imshow is the restored image of SL0, second imshow is the restored image of ℓ_2-SL0, third imshow is the restored image of ℓ_p-RLS, while the last imshow is the restored image of proposed RWCGSL0.

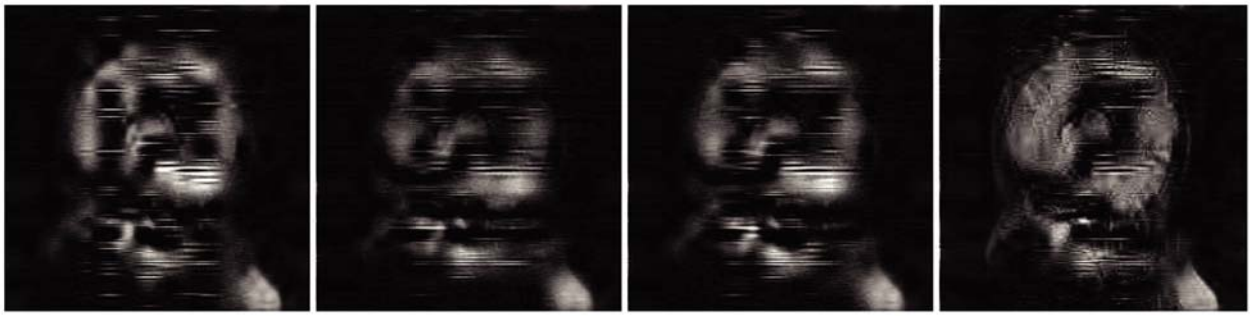

Figure 6. MR image recovery effect with $CR = 0.2$. From left to right, first imshow is the restored image of SL0, second imshow is the restored image of ℓ_2-SL0, third imshow is the restored image of ℓ_p-RLS, while the last imshow is the restored image of proposed RWCGSL0.

Figure 7. MR image recovery effect with $CR = 0.3$. From left to right, first imshow is the restored image of SL0, second imshow is the restored image of ℓ_2-SL0, third imshow is the restored image of ℓ_p-RLS, while the last imshow is the restored image of proposed RWCGSL0.

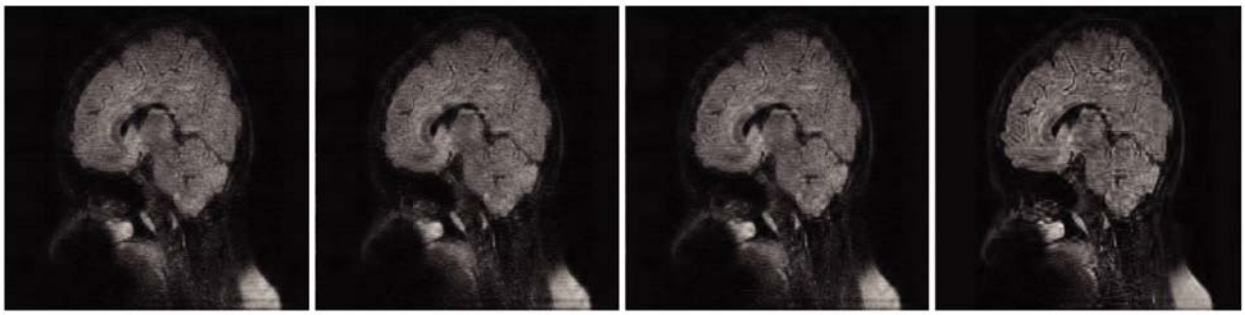

Figure 8. MR image recovery effect with $CR = 0.4$. From left to right, first imshow is the restored image of SL0, second imshow is the restored image of ℓ_2-SL0, third imshow is the restored image of ℓ_p-RLS, while the last imshow is the restored image of proposed RWCGSL0.

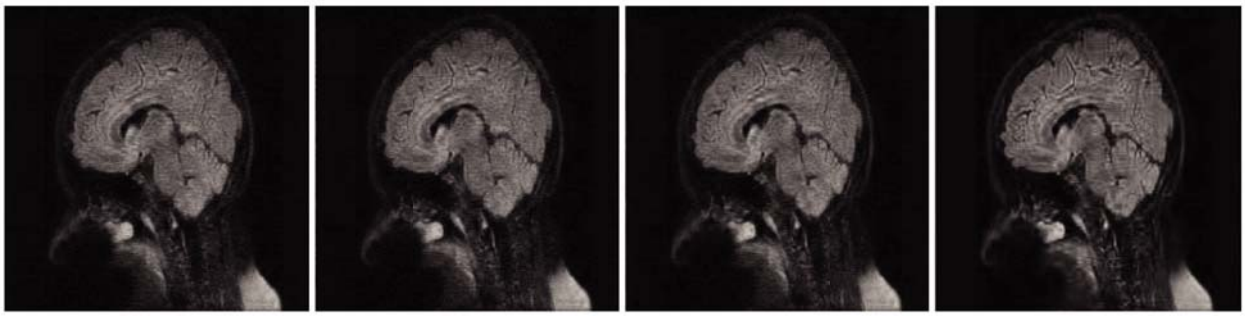

Figure 9. MR image recovery effect with $CR = 0.5$. From left to right, first imshow is the restored image of SL0, second imshow is the restored image of ℓ_2-SL0, third imshow is the restored image of ℓ_p-RLS, while the last imshow is the restored image of proposed RWCGSL0.

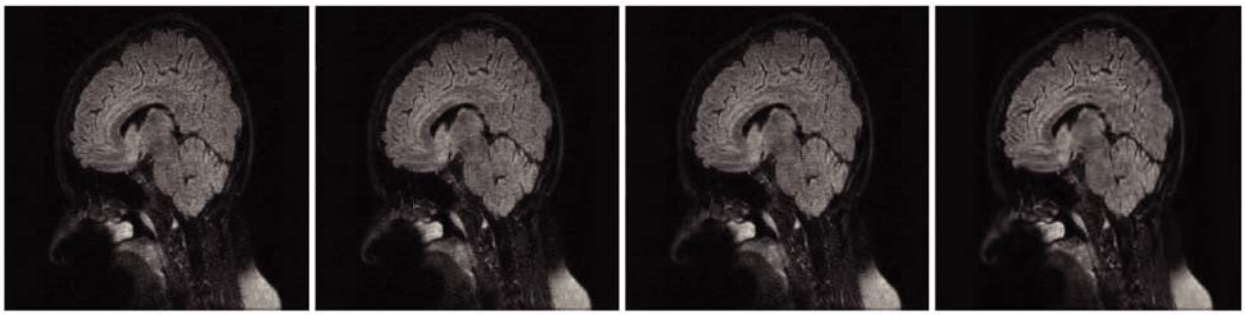

Figure 10. MR image recovery effect with $CR = 0.6$. From left to right, first imshow is the restored image of SL0, second imshow is the restored image of ℓ_2-SL0, third imshow is the restored image of ℓ_p-RLS, while the last imshow is the restored image of proposed RWCGSL0.

proposed RWCGSL0 algorithm are shown in Fig. 11 and Fig. 12, respectively. Meanwhile, scientific data are shown in Table 3.

Figure 12 shows anti-noise performance of the proposed RWCGSL0 algorithm when recovering MR images, while Fig. 11 shows the corresponding performance of the ℓ_p-RLS algorithm. It can be seen that when ξ is less than 0.2, the difference in MR image recovery of the proposed RWCGSL0 algorithm is not obvious, but when ξ is over 0.2, the effect of MR image recovery is significantly reduced, so is the ℓ_p-RLS algorithm. However, the RWCGSL0 algorithm performs better than the ℓ_p-RLS algorithm

Table 3. PSNR and SSIM of recovered MR images by the ℓ_p-RLS algorithm and the proposed RWCGSL0 algorithm at different ξ.

ξ	Algorithm	PSNR (dB)	SSIM (%)
0	RWCGSL0	29.0067	98.21
	ℓ_p-RLS	27.8262	97.64
0.05	RWCGSL0	27.6638	97.58
	ℓ_p-RLS	26.3769	96.76
0.1	RWCGSL0	23.1215	93.41
	ℓ_p-RLS	22.9231	93.11
0.2	RWCGSL0	18.8572	84.16
	ℓ_p-RLS	16.9773	77.25
0.5	RWCGSL0	7.7832	28.97
	ℓ_p-RLS	7.4864	28.07

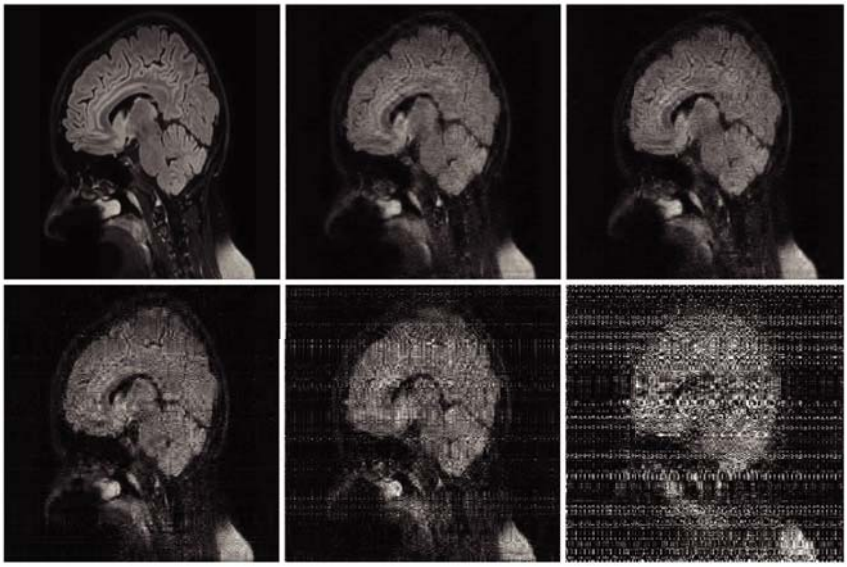

Figure 11. MR image recovery effect by ℓ_p-RLS algorithm when noise is incrementing according to a sequence $\xi = [0, 0.05, 0.1, 0.2, 0.5]$. And from left to right, from top to bottom, first imshow corresponds to the original image, second imshow is the restored image at the first level ($\xi = 0$), third imshow is the restored image at the second level ($\xi = 0.05$), fourth imshow is the restored image at the third level ($\xi = 0.1$), fifth imshow is the restored image at the fourth level ($\xi = 0.2$), while the last imshow is the restored image at the fifth level ($\xi = 0.5$).

under the same ξ. The scientific data in Table 3 also fully show it. These indicate that the proposed RWCGSL0 algorithm has denoising capability within a certain range of noise.

Through all the above experiments, we can conclude that the proposed RWCGSL0 algorithm has good signal recovery performance and can be successfully applied in MRI. Compared with state-of-the-art reconstruction approaches, RWCGSL0 algorithm has better MR image reconstruction accuracy on the basis that CS technology can accelerate the speed of MRI. The main reason is that the algorithm has advantages in three aspects: (1) the CGF can approximate the ℓ_0-norm well; (2) the combination of the weighting function and the CGF can promote sparsity; (3) the regularization mechanism has the ability to resist noise.

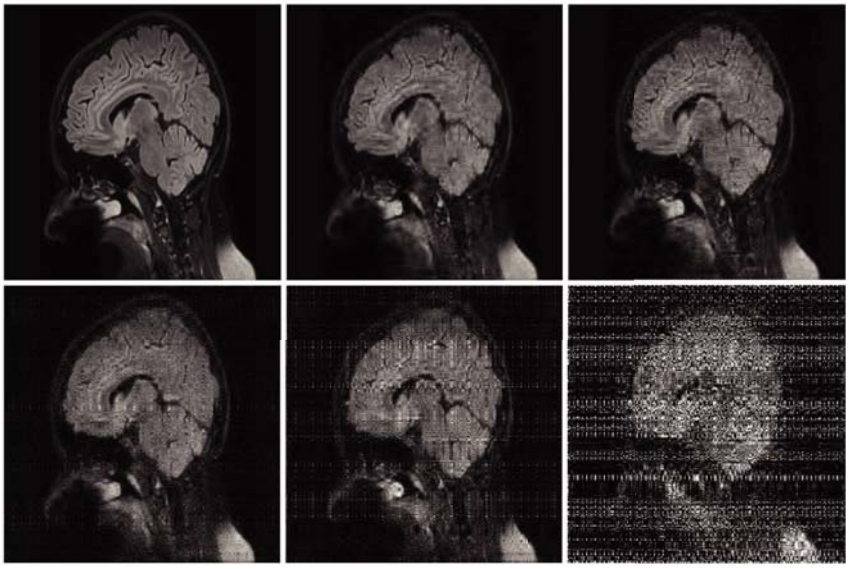

Figure 12. MR image recovery effect by proposed RWCGSL0 algorithm when noise is incrementing according to a sequence $\xi = [0, 0.05, 0.1, 0.2, 0.5]$. And from left to right, from top to bottom, first imshow corresponds to the original image, second imshow is the restored image at the first level ($\xi = 0$), third imshow is the restored image at the second level ($\xi = 0.05$), fourth imshow is the restored image at the third level ($\xi = 0.1$), fifth imshow is the restored image at the fourth level ($\xi = 0.2$), while the last imshow is the restored image at the fifth level ($\xi = 0.5$).

5. CONCLUSIONS

In this paper, we propose an RWCGSL0 algorithm that reconstructs MR images by a new smoothed function, weighting strategy, and regularization mechanism. The optimal solution of the algorithm's objective function framework is obtained by PD method. Further, the performance of the RWCGSL0 algorithm is verified by comparing with SL0, ℓ_2-SL0, ℓ_p-RLS algorithms. The experimental results show that the RWCGSL0 approach performs well in fast and accurate reconstruction of MR images and is superior to other popular approaches. In addition, testing the RWCGSL0 algorithm on different applications is our future work.

ACKNOWLEDGMENT

This paper is supported by the National Key Laboratory of Communication Anti-jamming Technology.

APPENDIX A. PROOF OF THEOREM 1.

Proof of Theorem 1. By the assumption $0 \in \chi_i$ for all i and the definitions of $\mathbf{x}^*$, $\tilde{\mathbf{x}}^*$ and $\mathbf{I}^*$, we clearly see that $\mathbf{x}^* \in \chi_1 \times \ldots \times \chi_n$ and $||\mathbf{x}^*||_0 \leq r$. Hence, $\mathbf{x}^*$ is a feasible solution of Eq. (6). It remains to show that $\phi(\mathbf{x}) \geqslant \phi(\mathbf{x}^*)$ for any feasible point $\mathbf{x}$ of Eq. (6). Indeed, let $\mathbf{x}$ be arbitrarily chosen such that $||\mathbf{x}||_0 \leqslant r$ and $\mathbf{x} \in \chi_1 \times \ldots \times \chi_n$, and let $\mathbf{J} = \{i | x_i \neq 0\}$. Clearly, $|\mathbf{J}| \leqslant r = |\mathbf{I}^*|$. Let $\bar{\mathbf{I}}^*$ and $\bar{\mathbf{J}}$ denote the complement of $\mathbf{I}^*$ and $\mathbf{J}$, respectively. It then follows that $|\bar{\mathbf{J}} \cap \mathbf{I}^*| = |\mathbf{I}^*| - |\mathbf{I}^* \cap \mathbf{J}| \geqslant |\mathbf{J}| - |\mathbf{I}^* \cap \mathbf{J}| = |\mathbf{J} \cap \bar{\mathbf{I}}^*|$. In view of the definitions of $\mathbf{x}^*$, $\mathbf{I}^*$, $\bar{\mathbf{I}}^*$, $\mathbf{J}$ and $\bar{\mathbf{J}}$, we further have

$$\begin{aligned}\phi(\mathbf{x}) - \phi(\mathbf{x}^*) \;=\; & \sum\nolimits_{i \in \mathbf{J} \cap \mathbf{I}^*} (\phi_i(x_i) - \phi_i(x_i^*)) + \sum\nolimits_{i \in \bar{\boldsymbol{J}} \cap \bar{\boldsymbol{I}}^*} (\phi_i(x_i) - \phi_i(x_i^*)) \\ & + \sum\nolimits_{i \in \bar{\boldsymbol{J}} \cap \mathbf{I}^*} (\phi_i(x_i) - \phi_i(x_i^*)) + \sum\nolimits_{i \in \mathbf{J} \cap \bar{\boldsymbol{I}}^*} (\phi_i(x_i) - \phi_i(x_i^*)),\end{aligned}$$

$$\geq \sum\nolimits_{i\in \bar{\boldsymbol{J}}\cap \mathbf{I}^*} (\phi_i(0)-\phi_i(x_i^*)) + \sum\nolimits_{i\in \mathbf{J}\cap \bar{\boldsymbol{I}}^*} (\phi_i(x_i^*)-\phi_i(0)),$$
$$= \sum\nolimits_{i\in \bar{\boldsymbol{J}}\cap \mathbf{I}^*} (\phi_i(0)-\phi_i(x_i^*)) + \sum\nolimits_{i\in \mathbf{J}\cap \bar{\boldsymbol{I}}^*} (\phi_i(0)-\phi_i(x_i^*)),$$

where the last inequality follows from the definition of $\mathbf{I}^*$ and the relation $|\bar{\mathbf{J}}\cap\mathbf{I}^*| \geqslant |\mathbf{J}\cap\bar{\mathbf{I}}^*|$. Thus, we see that $\phi(\mathbf{x}) \geqslant \phi(\mathbf{x}^*)$ for any feasible point $\mathbf{x}$ of Eq. (6), which implies that the conclusion holds [26].

REFERENCES

1. Shrividya, G. and S. H. Bharathi, "Application of compressed sensing on magnetic resonance imaging: A brief survey," *IEEE International Conference on Recent Trends in Electronics, Information & Communication Technology*, 2037–2041, 2017.
2. Donoho, D. L., "Compressed sensing," *IEEE Transactions on Information Theory*, Vol. 52, No. 4, 1289–1306, 2006.
3. Badeńska, A. and L. Błaszczyk, "Compressed sensing for real measurements of quaternion signals," *Journal of the Franklin Institute*, Vol. 354, No. 13, 5753–5769, 2017.
4. Candès, E. J. and M. B. Wakin, "An introduction to compressive sampling," *IEEE Signal Processing Magazine*, Vol. 25, No. 2, 21–30, 2008.
5. Lang, C., H. Li, G. Li, and X. Zhao, "Combined sparse representation based on curvelet transform and local DCT for multi-layered image compression," *IEEE International Conference on Communication Software and Networks*, Vol. 220, No. 6, 316–320, 2011.
6. Candès, E. J., J. Romberg, and T. Tao, "Robust uncertainty principles: Exact signal reconstruction from highly incomplete frequency information," *IEEE Transactions on Information Theory*, Vol. 52, No. 2, 489–509, 2006.
7. Tropp, J. A. and A. C. Gilbert, "Signal recovery from random measurements via orthogonal matching pursuit," *IEEE Transactions on Information Theory*, Vol. 53, No. 12, 4655–4666, 2007.
8. Jian, W., K. Seokbeop, and S. Byonghyo, "Generalized orthogonal matching pursuit," *IEEE Transactions on Signal Processing*, Vol. 60, No. 12, 6202–6216, 2012.
9. Needell, D. and J. A. Tropp, "CoSaMP: Iterative signal recovery from incomplete and inaccurate samples," *Applied & Computational Harmonic Analysis*, Vol. 26, No. 3, 301–321, 2009.
10. Dai, W. and O. Milenkovic, "Subspace pursuit for compressive sensing signal reconstruction," *IEEE Transactions on Information Theory*, Vol. 55, No. 5, 2230–2249, 2009.
11. Chen, S. S., D. L. Donoho, and M. A. Saunders, "Atomic decomposition by basis pursuit," *SIAM Review*, Vol. 43, No. 1, 129–159, 2001.
12. Zhai, Y., J. Gan, Y. Xu, and J. Zeng, "Fast sparse representation for Finger-Knuckle-Print recognition based on smooth L_0 norm," *IEEE International Conference on Signal Processing*, 1587–1591, 2013.
13. Xiao, J., C. R. Del-Blanco, C. Cuevas, and N. García, "Fast image decoding for block compressed sensing based encoding by using a modified smooth l_0-norm," *IEEE International Conference on Consumer Electronics*, 234–236, 2016.
14. Wang, H., Q. Guo, G. Zhang, G. Li, and W. Xiang, "Thresholded smoothed ℓ_0 norm for accelerated sparse recovery," *IEEE Communications Letters*, Vol. 19, No. 6, 953–956, 2015.
15. Ghalehjegh, S. H., M. Babaie-Zadeh, and C. Jutten, "Fast block-sparse decomposition based on SL0," *International Conference on Latent Variable Analysis and Signal Separation*, 426–433, 2010.
16. Zhao, R., W. Lin, L. Hao, and A. H. Shaohai, "Reconstruction algorithm for compressive sensing based on smoothed l_0 norm and revised newton method," *Journal of Computer-Aided Design & Computer Graphics*, Vol. 24, No. 4, 478–484, 2012.
17. Ye, X., W. P. Zhu, A. Zhang, and J. Yan, "Sparse channel estimation of MIMO-OFDM systems with unconstrained smoothed l_0-norm-regularized least squares compressed sensing," *Eurasip Journal on Wireless Communications & Networking*, Vol. 2013, No. 1, 282, 2013.

18. Ye, X. and W. P. Zhu, "Sparse channel estimation of pulse-shaping multiple-input-multiple-output orthogonal frequency division multiplexing systems with an approximate gradient l_2-l_0 reconstruction algorithm," *Iet Communications*, Vol. 8, No. 7, 1124–1131, 2014.
19. Soussen, C., J. Idier, J. Duan, and D. Brie, "Homotopy based algorithms for l_0-regularized least-squares," *IEEE Transactions on Signal Processing*, Vol. 63, No. 13, 3301–3316, 2015.
20. Yin, W., D. Goldfarb, and S. Osher, "The total variation regularized $Lsp1$ model for multiscale decomposition," *Siam Journal on Multiscale Modeling & Simulation*, Vol. 6, No. 1, 190–211, 2013.
21. Pant, J. K., W. S. Lu, and A. Antoniou, "New improved algorithms for compressive sensing based on ℓ_p norm," *IEEE Transactions on Circuits & Systems II Express Briefs*, Vol. 61, No. 3, 198–202, 2014.
22. Malek-Mohammadi, M., A. Koochakzadeh, M. Babaie-Zadeh, M. Jansson, and C. R. Rojas, "Successive concave sparsity approximation for compressed sensing," *IEEE Transactions on Signal Processing*, Vol. 64, No. 21, 5657–5671, 2016.
23. Li, S., H. Yin, and L. Fang, "Remote sensing image fusion via sparse representations over learned dictionaries," *IEEE Transactions on Geoscience & Remote Sensing*, Vol. 51, No. 9, 4779–4789, 2013.
24. Zhang, J., D. Zhao, F. Jiang, and W. Gao, "Structural group sparse representation for image compressive sensing recovery," *IEEE International Conference on Data Compression*, 331–340, 2013.
25. Hawes, M. B. and W. Liu, "Robust sparse antenna array design via compressive sensing," *International Conference on Digital Signal Processing*, 1–5, 2013.
26. Lu, Z. and Y. Zhang, "Penalty decomposition methods for L_0-norm minimization," *Mathematics*, 2010.
27. Shi, Z., "A weighted block dictionary learning algorithm for classification," *Mathematical Problems in Engineering*, Vol. 2016, 2016.
28. Candés, E. J., M. B. Wakin, and S. P. Boyd, "Enhancing sparsity by reweighted L_1 minimization," *Journal of Fourier Analysis & Applications*, Vol. 14, No. 5–6, 877–905, 2008.
29. Rudin, L. I., S. Osher, and E. Fatemi, "Nonlinear total variation based noise removal algorithms," *Physica D Nonlinear Phenomena*, Vol. 60, No. 1–4, 259–268, 1992.
30. Wen, F., Y. Yang, P. Liu, R. Ying, Y. Liu, "Efficient ℓ_q minimization algorithms for compressive sensing based on proximity operator," *Mathematics*, 2016.